

PAPER • OPEN ACCESS

Conversion of a mixture of date palm wastes to mesoporous activated carbon for efficient dye adsorption

To cite this article: Hattan A Alharbi *et al* 2023 *Mater. Res. Express* **10** 015602

View the [article online](#) for updates and enhancements.

You may also like

- [Ab initio studies on the optical effects in the deep ultraviolet nonlinear optical crystals of the \$\text{KBe}_2\text{BO}_3\text{F}_2\$ family](#)
Lei Kang, Siyang Luo, Hongwei Huang et al.
- [Evaluation of blackbody radiation shift with \$2 \times 10^{-18}\$ uncertainty at room temperature for a transportable \$^{40}\text{Ca}^+\$ optical clock](#)
Ping Zhang, Jian Cao, Jin-bo Yuan et al.
- [Immobilization of *Trametes hirsuta* D7 in Light Expanded Clay Aggregate for Decolorization of Synthetic Dye](#)
F C Ardiati, D H Y Yanto, S H Anita et al.



EDINBURGH INSTRUMENTS

WORLD LEADING MOLECULAR SPECTROSCOPY SOLUTIONS

edinst.com

The advertisement features a red background with the Edinburgh Instruments logo on the left, which consists of a stylized sunburst pattern. Below the logo, the text 'WORLD LEADING MOLECULAR SPECTROSCOPY SOLUTIONS' is written in white. On the right side, there are several pieces of laboratory equipment, including a large white instrument labeled 'FLS 1000' and a smaller one labeled 'FSS'. The website 'edinst.com' is displayed in a white box in the bottom right corner.

Materials Research Express



PAPER

Conversion of a mixture of date palm wastes to mesoporous activated carbon for efficient dye adsorption

OPEN ACCESS

RECEIVED

27 September 2022

REVISED

1 January 2023

ACCEPTED FOR PUBLICATION

12 January 2023

PUBLISHED

25 January 2023

Original content from this work may be used under the terms of the [Creative Commons Attribution 4.0 licence](https://creativecommons.org/licenses/by/4.0/).

Any further distribution of this work must maintain attribution to the author(s) and the title of the work, journal citation and DOI.



Hattan A Alharbi¹ , Bassim H Hameed², Khaled D Alotaibi^{3,*} , Saud S Al-Oud³ and Abdullah S Al-Modaihsh³

¹ Department of Plant Protection, College of Food and Agriculture Sciences, King Saud University, PO Box 2460, Riyadh 11451, Saudi Arabia

² Department of Chemical Engineering, College of Engineering, Qatar University, PO Box 2713, Doha, Qatar

³ Department of Soil Science, College of Food and Agriculture Sciences, King Saud University, PO Box 2460, Riyadh 11451, Saudi Arabia

* Author to whom any correspondence should be addressed.

E-mail: khalotaibi@ksu.edu.sa

Keywords: activated carbon, reactive dyes, phoenix dactylifera l., isotherm, kinetic, hydrothermal carbonization

Abstract

In this study, we aimed to develop mixture activated carbon (MAC) from a mixture of date palm wastes (petiole, rachis and fiber) through hydrothermal carbonization and microwave-assisted H_3PO_4 activation and evaluate its adsorption capacity to remove Remazol brilliant blue R (RBBR) from aqueous solution. The MAC was found to be mesoporous, with an average pore diameter and BET surface area of 2.61 nm and $641.23 \text{ m}^2 \text{ g}^{-1}$, respectively. The zeta potential and FTIR results demonstrated that the surface of MAC was negatively charged in its natural state and filled with functional groups such as phenyl, secondary amine, alkyne, aldehyde, and hydroxy groups. The adsorption capacity and percentage removal of RBBR increased and decreased, respectively, when the initial concentration increased. Maximum removal of RBBR was achieved at pH 3 (96.69 mg g^{-1}) and at 30°C of solution temperature (85.79 mg g^{-1}). Langmuir and pseudo-first-order were the best isotherm and kinetic models for describing the RBBR-MAC adsorption system, respectively. The thermodynamic parameters of ΔH° , ΔS° , ΔG° , and E_a implied that this adsorption system was exothermic, increased randomness at the liquid-solid interface, and was spontaneous and controlled by the physisorption type of sorption, respectively.

1. Introduction

Products with color finishing have a higher market value and demand than those without. Therefore, the production of dyes is increasing to satisfy the needs of several industries, including textiles, books, magazines, household products, cosmetics, and foods (Mahapatra *et al* 2021, Mohamad *et al* 2022). However, these industries have the potential to discharge wastewater containing dyes above permissible levels into the environment (Yaseen and Scholz 2019). According to Varjani *et al* (2020) and Guo *et al* (2020), as much as 2.15×10^9 tons of dye wastewater is discharged by the textile industry annually. Remazol brilliant blue R (RBBR) is one of the most commonly used dyes and belongs to the reactive anionic class. Yusop *et al* (2022a) stated that such a class of dyes is more difficult to remove from water than the other classes because of the former's ability to dissolve in water to produce negative ions attracted to the positive end of water molecules. Most reactive dyes, including RBBR, can be characterized by a minimum azo bond ($-N=N-$) in their structure. According to Sharma *et al* (2021), reactive dyes require serious attention because their discharge into the environment has reached 10%–50%. The interaction between RBBR and living organisms, including humans, can cause serious health problems owing to its toxicity and carcinogenicity (Zhang *et al* 2022).

Among the technologies developed to solve the dye wastewater problem, adsorption processes using activated carbon (AC) have produced the best results owing to the following advantages: (i) they are versatile in adsorbing different types of pollutants such as dyes (Ahmad *et al* 2017, Ahmad *et al* 2021), heavy metals (Yusop *et al* 2022b), phenolic compounds (Aldawsari *et al* 2020), and pesticides (Aziz *et al* 2021) (ii) they can be derived

from renewable agricultural wastes, namely, durian peel (Yusop *et al* 2021), *Alpinia galanga* stem (Ahammad *et al* 2021), and acacia sawdust (Yusop *et al* 2017); (iii) they have a relatively simple design and process (Shahbazi *et al* 2020); and (iv) they are economically feasible.

One of the most planted trees in the Middle East and North African countries is the date palm (*Phoenix dactylifera* L.), which belongs to the *Arecaceae* family. This ancient tree is cultivated for its fruits, and its other parts have limited use. Throughout the literature, wastes from parts of date palms have been successfully converted to AC to adsorb pollutants. For instance, Aichour *et al* (Aichour 2022) studied the removal of anionic dyes by date palm petiole-based AC; Daoud *et al* (2017) utilized date palm rachis as AC to remove dye; and Melliti *et al* (2021) produced date palm fiber-based AC to adsorb tylosin antibiotics.

Therefore, the aim of this study was to convert a mixture of date palm petiole (DPP), date palm rachis (DPR), and date palm fiber (DPF) into AC (MAC) via a hydrothermal carbonization process, followed by phosphoric acid treatment and microwave heating, and evaluate its adsorption capacity to remove RBBR from aqueous solutions. The microwave irradiation technique was adopted because it activates the sample at a faster rate owing to its natural working principle of converting electromagnetic waves into thermal energy on a volumetric scale (Omoriyekomwan *et al* 2021).

2. Materials and method

2.1. Materials

The precursors of DPP, DPR, and DPF were collected from a date palm farm near Riyadh, Saudi Arabia. Phosphoric acid, H_3PO_4 (purchased from Sigma Aldrich), 0.10 M hydrochloric acid, HCl (purchased from R&M Chemicals), and RBBR dye in powder form (supplied by Merck) were used.

2.2. Preparation of date palm wastes mixture-based AC (MAC)

The collected DPP, DPR, and DPF were dried in open air, chopped into small pieces, and thoroughly washed with tap water to remove dirt and impurities. Next, they were dried in an oven at 110 °C for 2 d, after which these precursors were finely ground to a particle size from 1 to 2 mm. Subsequently, ground DPP, DPR, and DPF were mixed at a mass ratio of 1:1:1. Afterward, the mixture was carbonized via the hydrothermal carbonization method at 200 °C for 5 h and at a heating rate of 5 °C min⁻¹. The resulting sample was labeled hydrochar. The hydrochar was then impregnated with H_3PO_4 for 8 h at a weight impregnation ratio (IR) of 1:3. Subsequently, the impregnated sample was activated in a microwave oven (EMW2001W, Sweden) by employing 616 Watt of radiation power and 10 min of radiation time with inert gas N_2 (99.9% purity) flowing through the samples at 80 cm³ min⁻¹. Subsequently, the activated sample was soaked in 0.10 M HCl for 30 min under stirring. Later, the soaked sample was washed with warm water until a pH value between 6 and 7 was acquired for the washing solution. Washed samples were dried at 50 °C for 2 d. The dried sample was labeled date palm waste-mixture-based AC (MAC). MAC was stored in an airtight box to be used in the adsorption study.

2.3. Characterization methods

Several characterizations were conducted on the samples: (i) BET surface area, Langmuir surface area, total pore volume, and average pore size using a volumetric adsorption analyzer (Micromeritics ASAP 2020); (ii) scanning electron microscopy (SEM) using a scanning electron microscope (Model: LEO SUPRA 55VP, Germany); (iii) elemental analysis using a simultaneous thermal analyzer (STA; Model: Model Perkin Elmer STA 6000, USA); (iv) proximate analysis using thermogravimetric analysis (TGA); (v) functional groups spectrum using a Fourier transform infrared spectroscopy (Model: IR Prestige 21 Shimadzu, Japan); and (vi) zeta potential distribution using a zeta potential analyzer (Model: Zetasizer Nano Series DKSH).

2.4. Equilibrium study

An equilibrium study was conducted to verify the effect of several parameters on the performance of MAC for adsorbing RBBR dye. The first parameter studied was the initial RBBR concentration. RBBR solutions with six different known concentrations (25–300 mg l⁻¹) were produced and kept inside Erlenmeyer flasks, which were later placed in a water bath shaker. A precisely weighed 0.2 g MAC was added to each of these conical flasks to allow the adsorption process to occur. Other conditions, such as rotation speed, solution temperature, solution pH, and solution volume, were fixed at 60 rpm, 30 °C, original pH, and 200 ml, respectively. The concentration of the RBBR solution was quantified at a wavelength of 590 nm using UV–vis spectrophotometry (Model: Agilent Cary 60, USA) every 30 min until the equilibrium phase was attained. The second parameter studied was the effect of the solution temperature. The temperatures of the RBBR solution were altered to 30, 40, and 50 °C, and the solution pH remained in its original state with no alterations. The third parameter studied was the effect of solution pH, where the pH of RBBR solutions was adjusted to 3, 5, 7, 9, 11, and 13 by adding NaOH or HCl.

Solution temperature was maintained at 30 °C. For both studies, other conditions, such as solution volume, adsorbent dosage, and rotation speed, were fixed at 200 ml, 0.2 g, and 60 rpm, respectively. The adsorption capacity and percentage removal of RBBR by MAC were determined using the following equations:

$$q_e = \frac{(C_o - C_e)V}{M} \quad (1)$$

$$\text{Removal (\%)} = \frac{(C_o - C_e)}{C_o} \times 100\% \quad (2)$$

where the quantity of RBBR molecules adsorbed by MAC in the equilibrium phase (mg/g), the RBBR concentration in the initial phase (mg/l), the RBBR concentration in the equilibrium phase (mg/l), solution volume (ml), and the amount of MAC used (g) are denoted by q_e , C_o , C_e , V , and M , respectively.

2.5. Isotherm study

Vital information related to the concentration of the adsorbate in the bulk and solid phases can be verified by performing isotherm studies. Therefore, the two most well-known isotherm models, Langmuir and Freundlich, were used, and their respective formulas are as follows:

Langmuir (Langmuir 1918):

$$q_e = \frac{Q_m K_L C_e}{1 + K_L C_e} \quad (3)$$

Freundlich (Freundlich 1906):

$$q_e = K_F C_e^{1/n_F} \quad (4)$$

where Q_m is the Langmuir maximum monolayer coverage (mg/g), K_L is the Langmuir constant associated with adsorption energy (L/mg), K_F is the adsorption constant of Freundlich (mg/g)(L/mg)^{1/n_F}, n_F is the heterogeneity factor, and R is the universal gas constant (8.314 J mol⁻¹. K), and T is the temperature of the solution (K).

Microsoft Excel Solver v. 2016 was used to solve the nonlinear isotherm models. The best isotherm model was determined based on the correlation coefficient, R^2 , with the root mean squared error (RMSE). RMSE can be calculated using the following formula (Marrakchi *et al* 2020):

$$RMSE = \sqrt{\frac{1}{n-1} \sum_n^{n=1} (q_{e,exp,n} - q_{e,cal,n})^2} \quad (5)$$

2.6. Kinetic study

The kinetic study was performed using the same procedure as that used in the equilibrium study. However, unlike in the equilibrium study, the RBBR concentration was measured at a fixed time between 0 and 180 min. Pseudo-first-order (PFO) and pseudo-second-order (PSO) were adopted to describe the kinetic data, and their formulas are as follows:

PFO (Lagergren 1898):

$$q_t = q_e [1 - \exp(-k_1 t)] \quad (6)$$

PSO (Ho and Mckay 1998):

$$q_t = \frac{k_2 q_e^2 t}{1 + k_2 q_e t} \quad (7)$$

where k_1 represents the rate constant for the PFO model (1/min), and k_2 denotes the rate constant for the PSO model (g/mg min). The best kinetic model was determined based on the RMSE values.

2.7. Thermodynamic study

Changes in the adsorption temperature have a significant effect on the adsorbate-adsorbate interaction in the adsorption process. Thus, a thermodynamic study was performed to determine the essential parameters of the change in enthalpy, ΔH° ; change in entropy, ΔS° ; Gibbs free energy, ΔG° ; and Arrhenius activation energy, E_a . The Van't Hoff equation was used to compute the values of ΔH° (kJ/mol) and ΔS° (kJ/mol). K). This equation is as follows:

$$\ln K_c = \frac{\Delta S^\circ}{R} - \frac{\Delta H^\circ}{RT} \quad (8)$$

where R is the gas constant (8.314 J mol⁻¹. K); T is the solution temperature (K); and K_c is the equilibrium constant (dimensionless), which can be calculated using the following formula (Lima *et al* 2019):

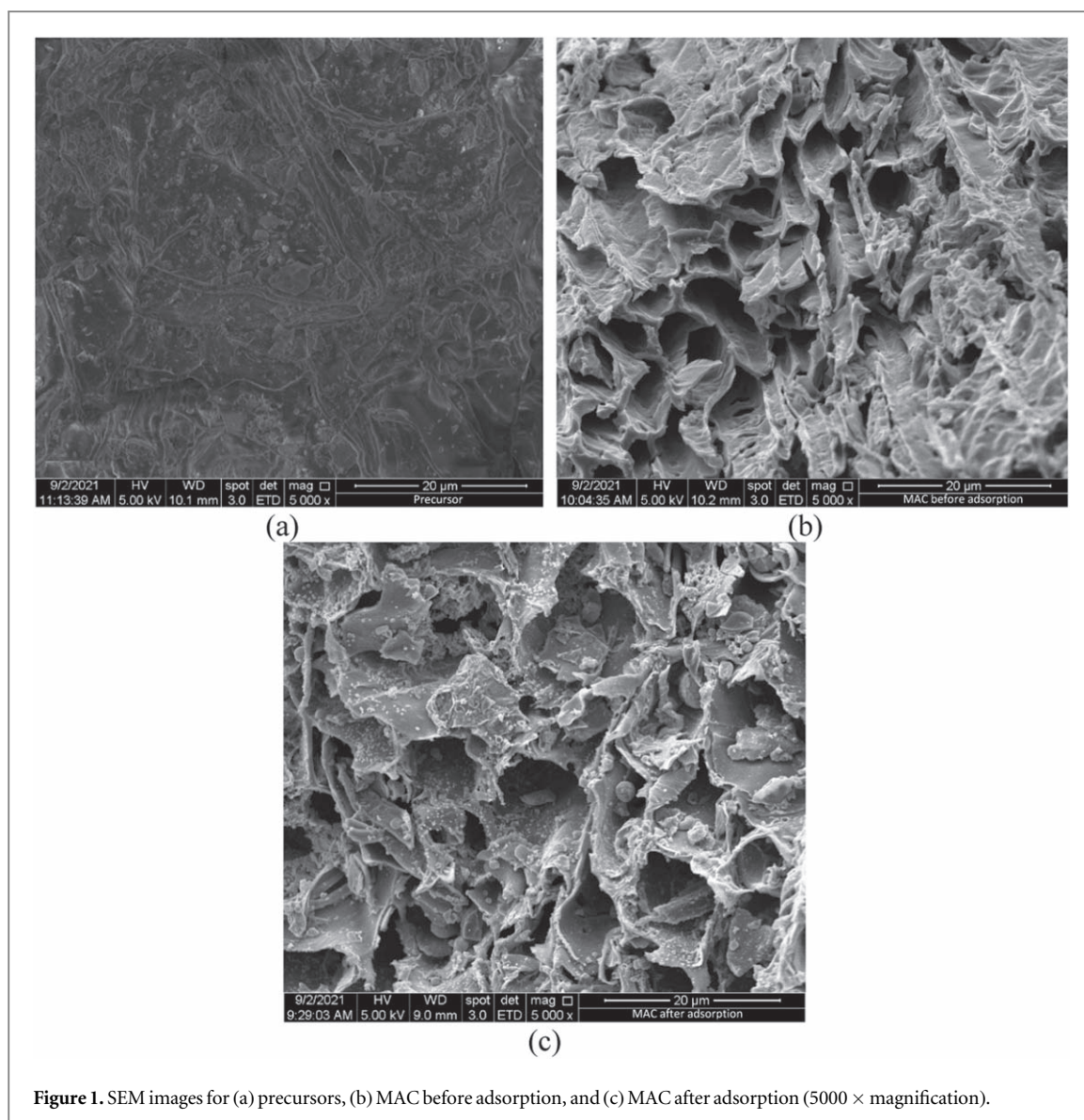


Figure 1. SEM images for (a) precursors, (b) MAC before adsorption, and (c) MAC after adsorption (5000 × magnification).

Table 1. Elemental and proximate analysis of samples.

Samples	Elemental analysis					Proximate analysis			
	C	H	N	S	Others	Moisture	Volatile matter	Fixed carbon	Ash
Mixture of precursors	37.40	7.15	1.36	1.41	52.68	8.98	65.91	19.44	5.68
MAC	58.42	3.33	1.39	0.01	36.85	6.35	13.35	79.24	1.05

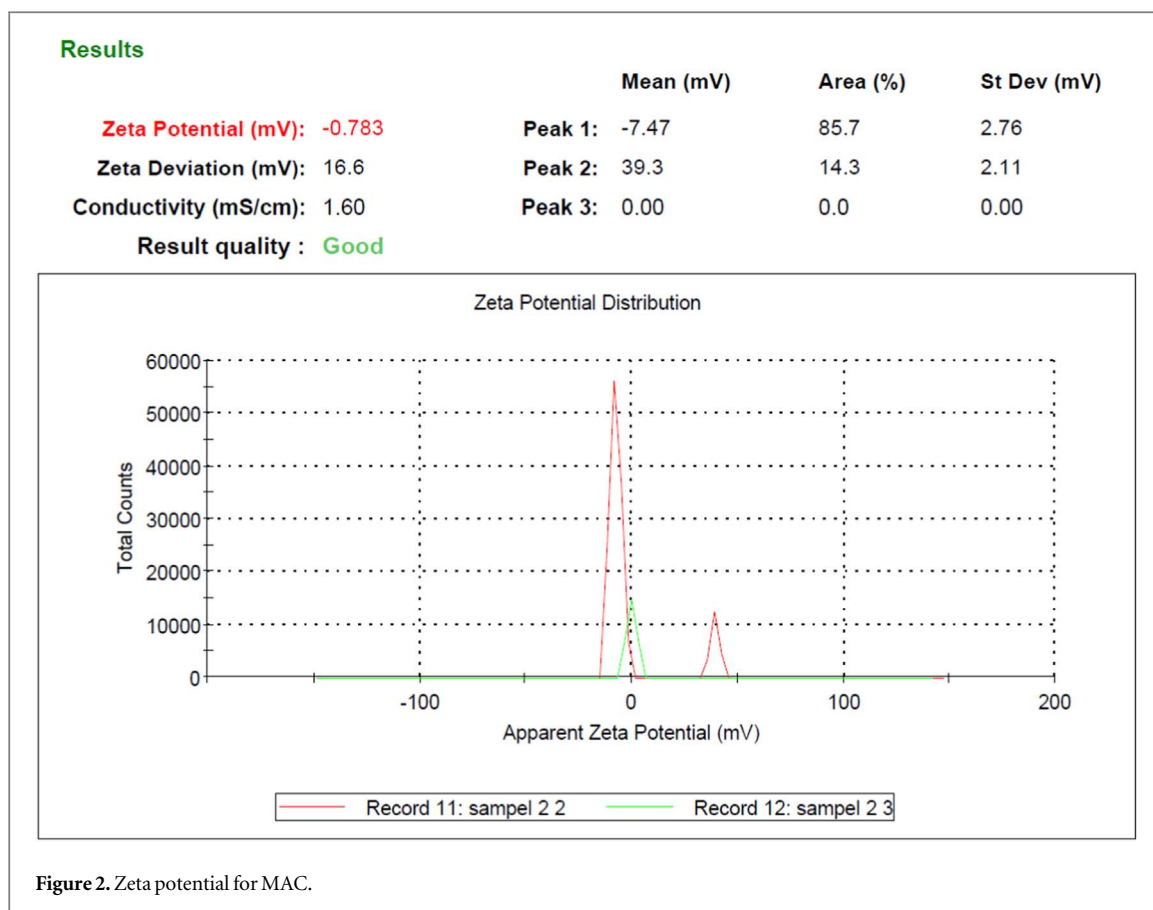
$$K_c = \frac{1000 \frac{mg}{g} \times K_L \times \text{molecular weight of adsorbate} \times [\text{adsorbate}]^\circ}{\gamma} \quad (9)$$

where $[\text{adsorbate}]^\circ$ is the standard concentration of adsorbate, and at the standard conditions, this value can be assumed as 1 mol L^{-1} ; γ is the adsorbate's activity coefficient (dimensionless); and K_L is the Langmuir adsorption constant (L/mg). The other two thermodynamic parameters, ΔG° (kJ/mol) and E_a (kJ/mol), were computed using the following formulas:

$$\Delta G^\circ = \Delta H^\circ - \Delta TS^\circ \quad (10)$$

$$\ln k_2 = \ln A - \frac{E_a}{RT} \quad (11)$$

where k_2 is the rate constant from PSO (g/mg min), and A is the Arrhenius factor.



3. Results and discussion

3.1. Characteristics of samples

BET surface area for MAC was $641.23 \text{ m}^2 \text{ g}^{-1}$, and this value is relatively moderate when compared with that of teak wood-based AC (AWAC), which posed $1345.25 \text{ m}^2 \text{ g}^{-1}$ (Yusop *et al* 2022a). Unlike MAC, which was synthesized using a microwave irradiation technique under the flow of inert N_2 gas, AWAC was produced using the same technique, but the activation gas of CO_2 was used. CO_2 gas bombarded the AWAC surface and created additional pores, explaining the higher BET surface area. In addition, the moderate BET surface area in MAC was caused by the lower radiation power of 616 W and shorter radiation time of 10 min applied during the MAC manufacturing process. Using the same chemical of H_3PO_4 acid for activation, Hijab *et al* (2021) created a date stone-based AC with a higher surface area ($1123 \text{ m}^2 \text{ g}^{-1}$) than those aforementioned owing to the higher radiation power of 850 W utilized in their study. A higher radiation power promotes a more aggressive volatilization process, effectively removing moisture, volatile matter, and tar compounds from the sample, creating a higher surface area. The formation of surface area in MAC was mainly attributed to H_3PO_4 acid, which optimized the degradation of polar cellulose and lignin components under microwave heating (Canales-Flores and Prieto-García 2020). MAC was confirmed to possess mesopore types of pores because the value obtained for average pore diameter was 2.61 nm. Mesopore-type pores were desired in this study for three main reasons: (i) sufficiently large to trap solid phase pollutants in wastewater, (ii) sufficiently small to create a higher surface area, and (iii) sufficiently small enough to prevent adsorbate loss (desorption) from occurring easily. The selection of H_3PO_4 as a chemical activating agent in this study was proven effective in creating mesopore pores in MAC, even at relatively low radiation power; similar findings have been reported by Han *et al* (2020) and Brazil *et al* (2022).

The results of the elemental and proximate analyses are presented in table 1. The precursors used in this study were found to have relatively high elemental C and fixed carbon percentages of 37.40% and 19.44%, respectively. After H_3PO_4 acid treatment and microwave heating, the percentages of elemental C and fixed carbon increased to 58.42% and 79.24%, respectively. By contrast, the other components of volatile matter, moisture, and ash decreased significantly from 65.91% to 13.35%, 8.98% to 6.35%, and 5.68% to 1.05%, respectively. During microwave heating, microwave energy causes electrons in polar moisture (water) and polar volatile matter (cellulose and lignin) to vibrate, producing heat that stimulates the evaporation process. Effective removal of these components was desired because their absence in the sample led to pore network generation.

Table 2. Summary of FTIR spectra for samples.

Precursor		MAC-BA		MAC-AA	
Bandwidth (cm ⁻¹)	Functional groups	Bandwidth (cm ⁻¹)	Functional groups	Bandwidth (cm ⁻¹)	Functional groups
1016	cyclohexane ring vibrations	731	C-H monosubstitution (phenyl)	957	aromatic C-H in-plane bend
1530	aromatic nitro compounds	961	trans-C-H out-of-plane bend	1072	cyclic ethers, C-O stretch
2100	C≡C terminal alkyne (monosubstituted)	1587	secondary amine, >N-H stretch bend	1177	secondary amine, CN stretch
3447	aromatic secondary amine, >N-H stretch	2100	C≡C terminal alkyne (monosubstituted)	1429	ammonium ions
3522	hydroxy group, H-bonded OH stretch	2727	aldehyde	1612	secondary amine, >N-H stretch bend
		3078	terminal C-H stretch	2110	C≡C terminal alkyne (monosubstituted)
		3200	hydroxy group, H-bonded OH stretch	3238	hydroxy group, H-bonded OH stretch

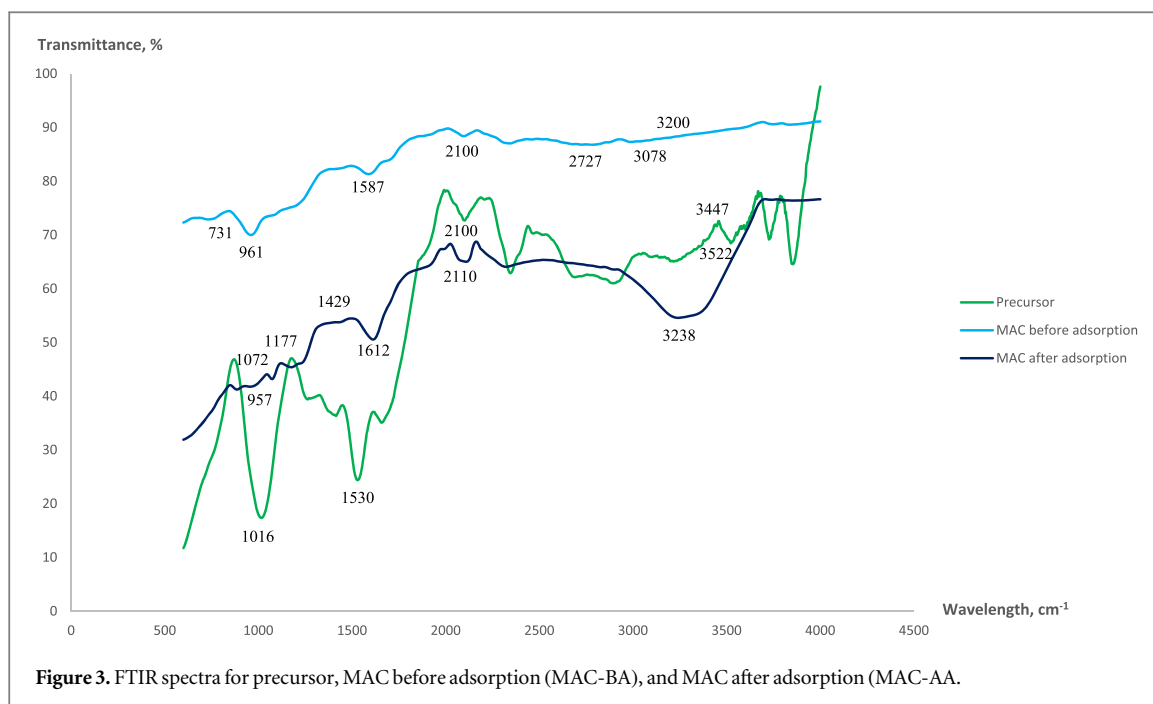


Figure 3. FTIR spectra for precursor, MAC before adsorption (MAC-BA), and MAC after adsorption (MAC-AA).

The surface morphologies of the precursor MAC before adsorption (MAC-BA) and MAC after adsorption (MAC-AA) were verified via SEM images, as shown in figures 1(a)–(c); based on these figures, no pores were detected on the surface of the precursor. By contrast, well-developed pores were observed on the surface of MAC-BA. These pores were successfully formed owing to the penetration of H_3PO_4 inside the skeleton of the carbon matrix structure of the sample coupled with microwave heating. As shown in figure 1(c), the molecules of RBBR dye fill the empty pores of MAC-AA. The type of sorption that binds between MAC-AA and RBBR can be determined in the next section of the isotherm, kinetic, and thermodynamic studies.

Depending on the type of raw materials and the activation technique applied, AC can carry a net charge on its surface. This net charge plays a major role in the adsorption process and can be directly reflected by the zeta potential value (Maršálek and Švidrnoch 2020). AC with a negative zeta potential value was more effective in removing positively charged adsorbates (Yusop *et al* 2022b). The zeta potential distribution for MAC is shown in figure 2, and its value was -0.783 mV. This negative value implies that the adsorption of RBBR onto MAC at the original pH of the RBBR solution was not boosted by electrostatic forces. Instead, repulsion occurred between the negatively charged MAC surface and the negatively charged RBBR ions.

Table 2 summarizes the bandwidths of the FTIR peaks and their respective functional groups. Figure 3 shows the FTIR spectra for the precursors MAC-BA and MAC-AA. The functional groups of $\text{C}\equiv\text{C}$ terminal alkyne (2100 , 2100 , and 2110 cm^{-1}) and the hydroxy group, H-bonded OH stretch (3522 , 3200 , and 3238 cm^{-1}), existed in all three samples of precursors MAC-BA and MAC-AA, respectively. However, functional groups such as cyclohexane ring vibrations (1016 cm^{-1}) and aromatic nitro compounds (1530 cm^{-1}) only appeared in the precursor. These compounds diminished in MAC-BA owing to their inability to survive H_3PO_4 chemical treatment and microwave heating. The activation technique applied in this study was observed to reduce aromatic secondary amine, $>\text{N}-\text{H}$ stretch in the precursor (3447 cm^{-1}) to secondary amine, $>\text{N}-\text{H}$ stretch bend (1587 cm^{-1}) in MAC-BA and secondary amine, and CN stretch (1177 cm^{-1}) in MAC-AA. New functional groups formed in MAC-BA, such as C-H monosubstitution (phenyl) (731 cm^{-1}), trans-C-H out-of-plane bend (961 cm^{-1}), aldehyde (2727 cm^{-1}), and terminal C-H stretch (3078 cm^{-1}). These new compounds resulted from the interaction between the original functional groups and H_3PO_4 acid, H_2O , and N_2 gas during microwave heating. After the adsorption process, the interaction between MAC-BA and RBBR was observed to create new functional groups of aromatic C-H-in-plane bend (957 cm^{-1}), cyclic ethers, C-O stretch (1072 cm^{-1}), and ammonium ions (1429 cm^{-1}).

3.2. Adsorption equilibrium

The effects of different initial RBBR concentrations and contact times on the adsorption capacity and removal percentage are shown in figures 4(a) and (b), respectively. Both plots reflect that the adsorption capacity and percentage removal of RBBR increased with time in the early phase of the adsorption process. After several hours, static points indicating equilibrium points were obtained. The equilibrium point is the point at which the MAC reached its exhaustion limit, and the net rate between the adsorption and desorption processes was equal

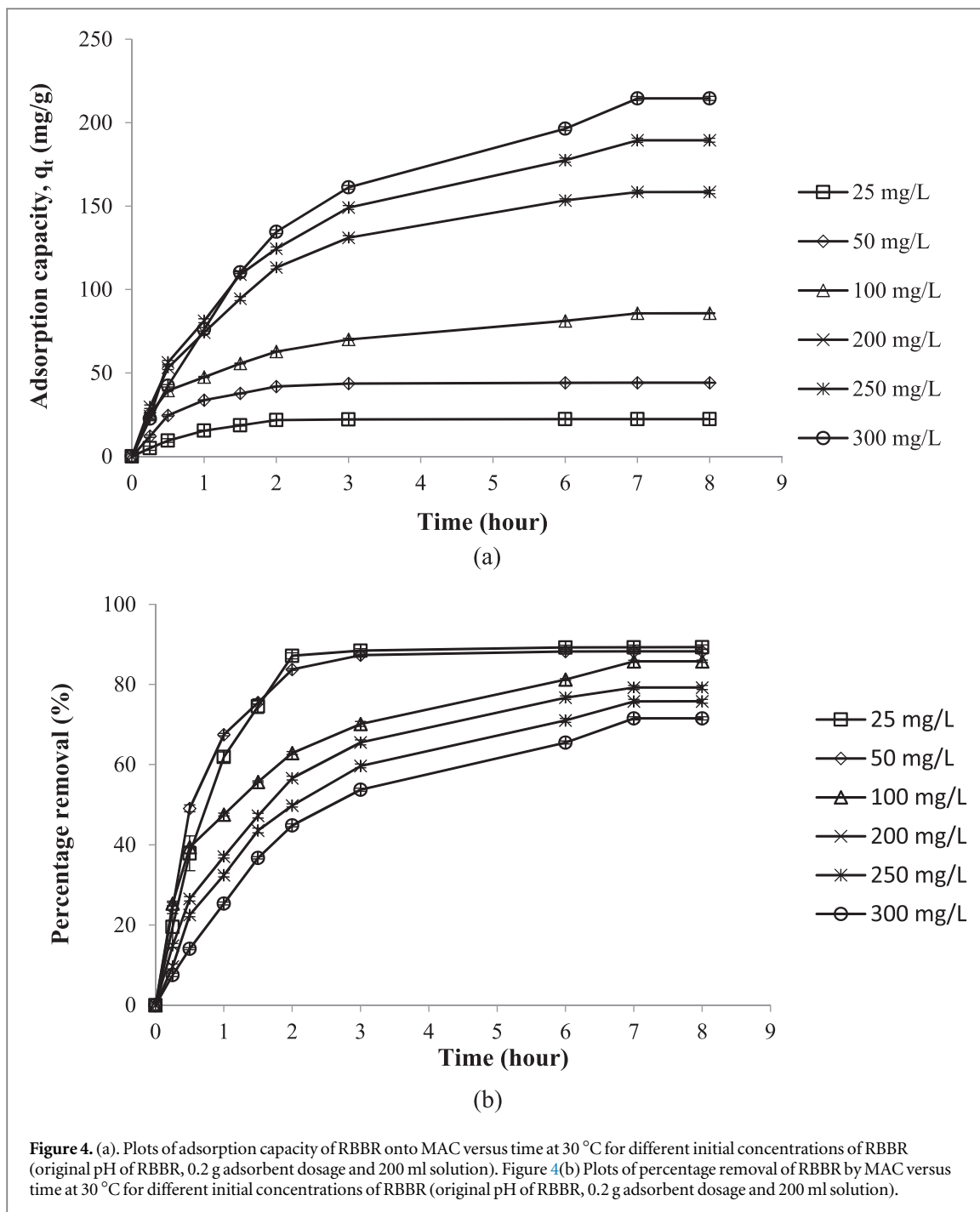
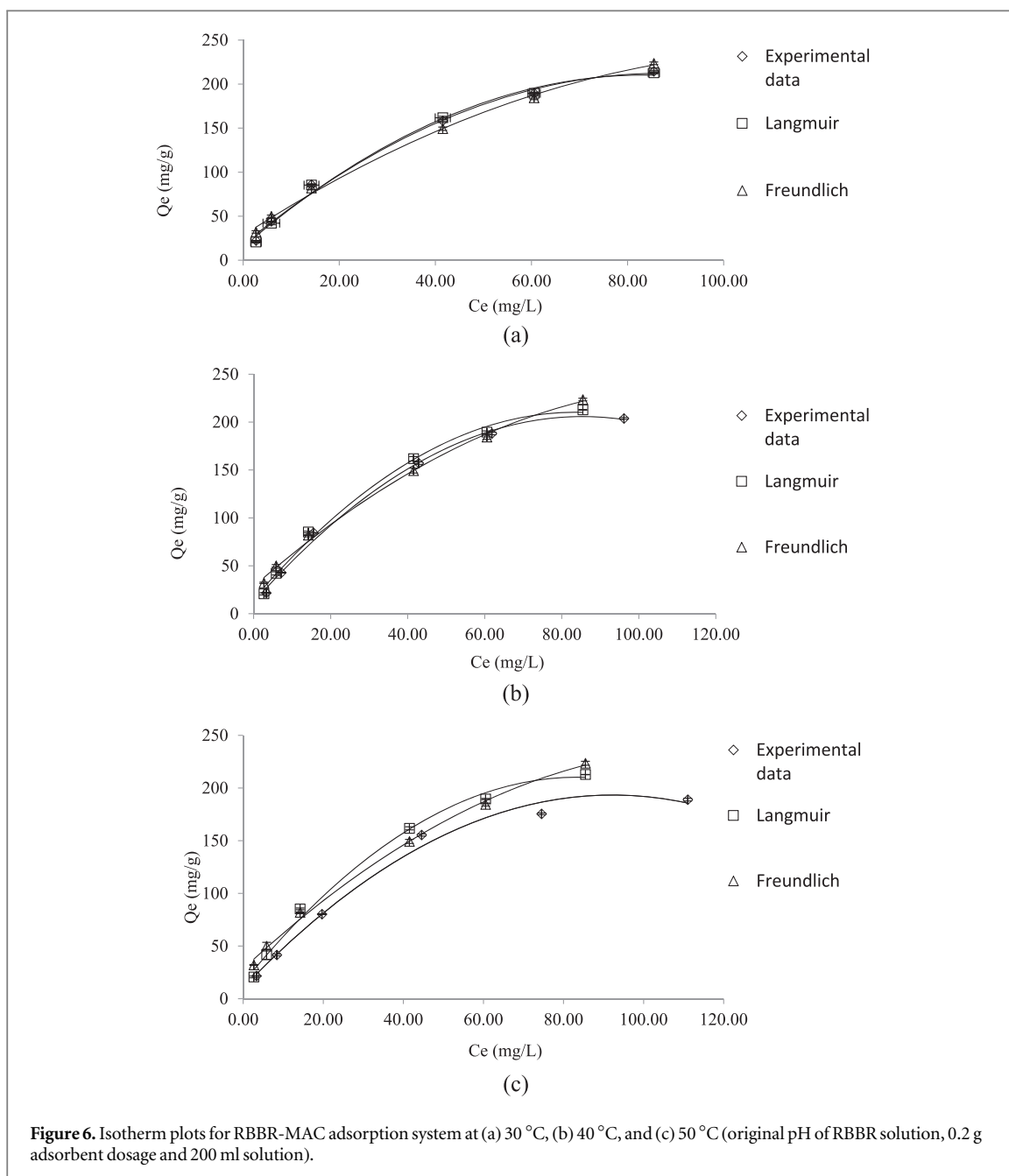
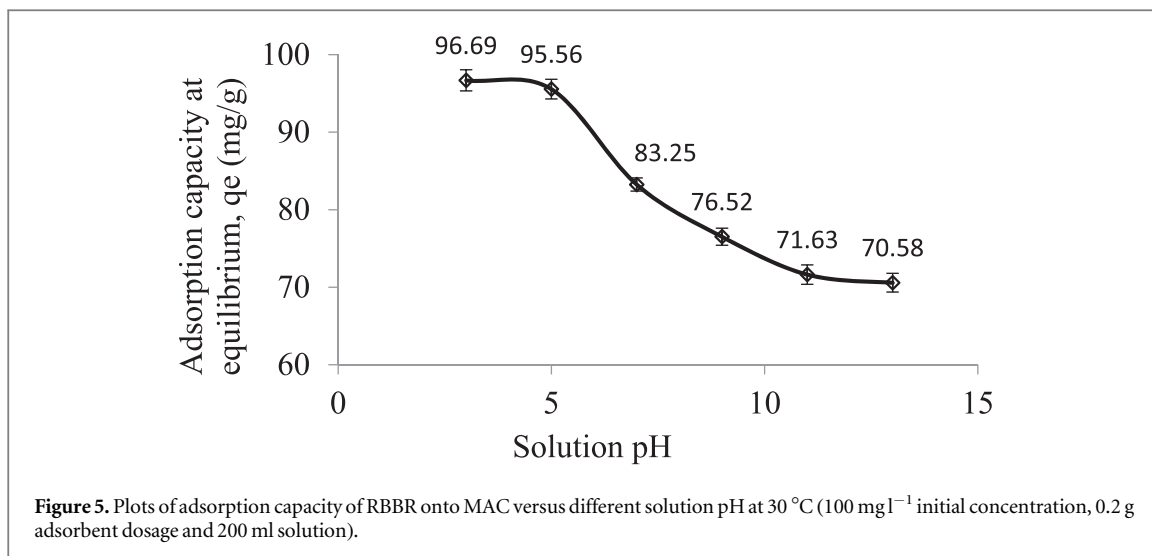
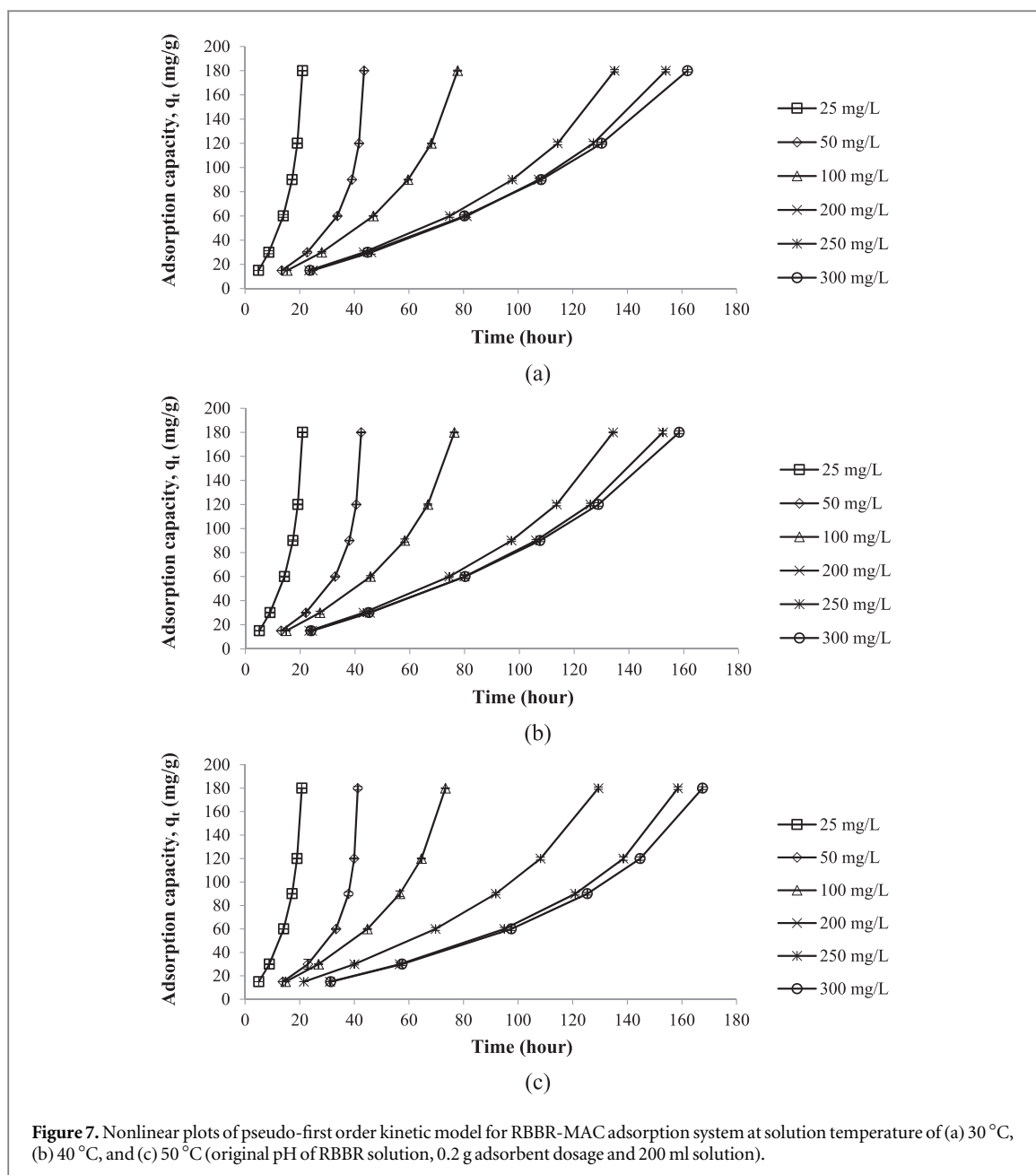


Table 3. Isotherm parameters for RBBR-MAC adsorption system.

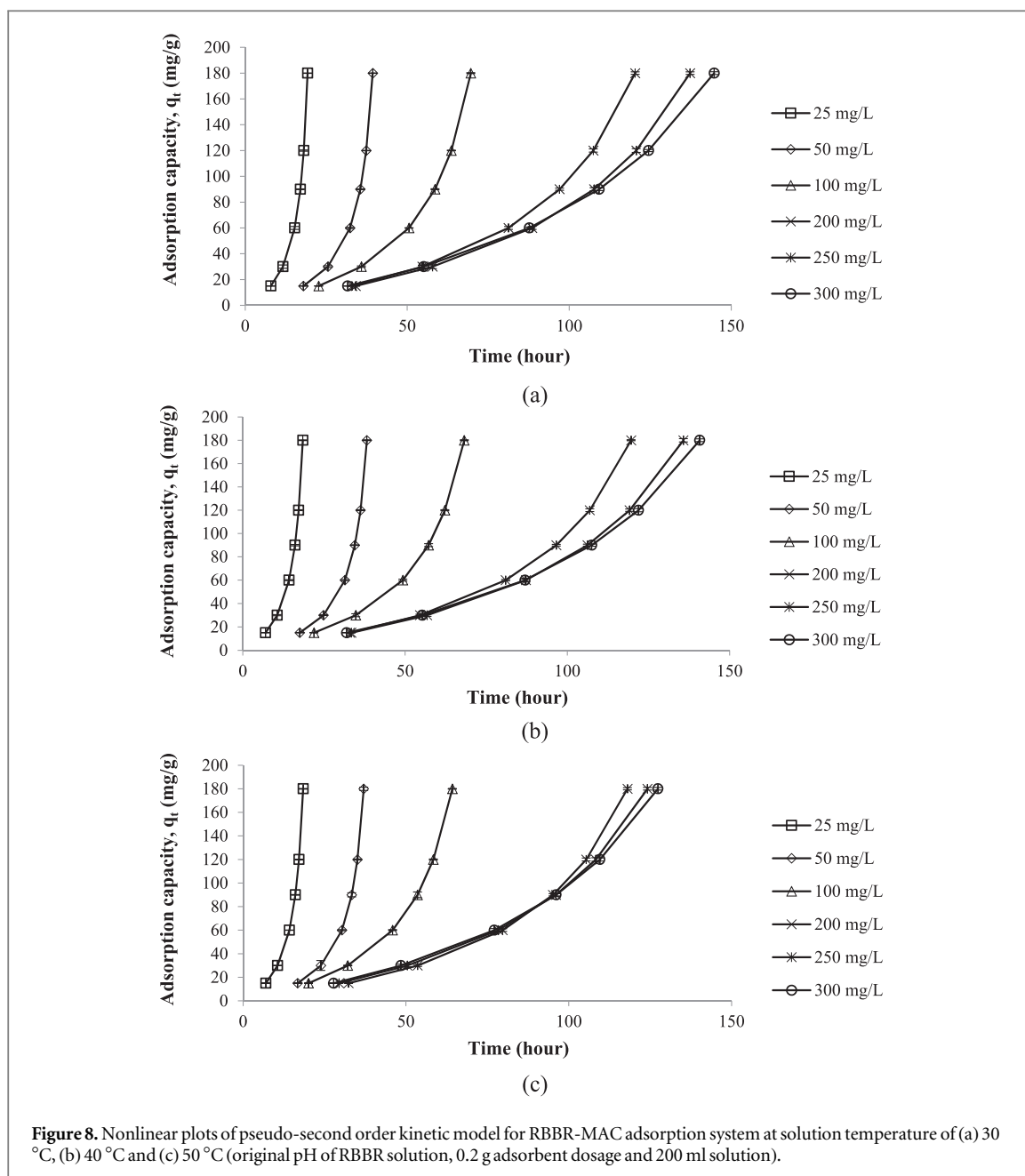
Isotherm	Parameters	30 °C	40 °C	50 °C
Langmuir	Q_m	303.14	284.87	263.92
	K_L	0.02755	0.02781	0.02585
	R^2	0.9945	0.9998	0.9903
	RMSE	1.87	4.84	7.67
Freundlich	K	18.61	19.13	18.09
	n	1.79	1.88	1.94
	R^2	0.9970	0.9966	0.9955
	RMSE	7.47	14.03	15.21





in magnitude. As shown in figure 4(a), an equilibrium phase was attained at a shorter time of 3 h for lower initial concentrations of 25 and 50 mg/l. Conversely, a longer time of 7 h was required at higher initial concentrations of 100, 200, 250, and 300 mg/l to achieve the same state. An explanation for this result is as follows: the higher the initial concentration, the higher the quantity of RBBR molecules, which increases the competition for adsorption site occupation, increasing the time for the equilibrium state to be attained. As shown in figure 4(b), as the RBBR initial concentration decreased from 300 to 25 mg l⁻¹, the percentage removal increased from 71.51% to 89.32%. At higher initial concentrations, the ratio of RBBR molecules to viable adsorption sites is high; therefore, an increased number of RBBR molecules cannot be adsorbed by MAC, reducing the removal percentage and vice versa.

The effect of solution pH on the RBBR-MAC adsorption system is shown in figure 5. High RBBR removal of 96.69 and 95.56 mg g⁻¹ was obtained at pH 3 and 5, respectively, confirming that RBBR removal was favored in acidic conditions. At pH values of 3 and 5, the solution was filled with excess H⁺ ions. These positive ions induced the surface of MAC to be positively charged, attracting negatively charged RBBR ions at a higher rate. At pH 7, a decrease in the adsorption capacity of 83.25 mg g⁻¹ was observed. Under this neutral condition, the adsorption of RBBR onto MAC was solely influenced by the original charge of the MAC surface, which was negative, verified by the zeta potential results in section 3.1. This negatively charged MAC surface created repulsion with negatively charged RBBR ions, explaining the decrease in RBBR adsorption capacity. Further



increases in the solution pH to 9, 11, and 13 reduced the RBBR adsorption capacity to 76.52, 71.63, and 70.58 mg g⁻¹, respectively. As the solution pH increased, the number of OH⁻ ions in the solution increased, inducing a negative charge on the MAC surface. The negatively charged MAC surface repulsed the negatively charged RBBR ions to a higher degree, resulting in a reduction in RBBR removal.

3.3. Adsorption isotherm

The Langmuir and Freundlich isotherm models were employed to fit the adsorption data; their parameters are summarized in table 3, and the isotherm plots are shown in figure 6. Based on table 3, the best model was Langmuir for describing the RBBR-MAC adsorption system, owing to its high R² value (>0.9903) and low RSME value (<7.67) for all ranges of solution temperatures studied. This signified that RBBR molecules formed monolayer coverage on the MAC's homogeneous surface with the maximum adsorption capacity, Q_m, of 303.14, 284.87, and 263.92 mg/g for solution temperatures of 30, 40, and 50 °C, respectively. This value is relatively high compared with that of RBBR removal by sewage sludge biochar, 126.59 mg g⁻¹ (Raj *et al* 2021); RBBR removal by acacia sawdust-based AC, 263.16 mg g⁻¹ (Yusop *et al* 2017); and RBBR removal by pomegranate peel-based AC, 20.34 mg g⁻¹ (Ahmad *et al* 2020). A reduction in the Q_m value as the solution temperature increased indicated that this adsorption process was exothermic in nature, which can be verified in the thermodynamic study in section 3.5. The exothermic nature of the adsorption process occurred because

Table 4. Kinetic parameters for RBBR-MAC adsorption system.

	Initial RBBR concentration (mg/L)	q_e , exp (mg/g)	Pseudo-first order (PFO)			Pseudo-second order (PSO)		
			q_e , cal (mg/g)	k_1 (min^{-1})	RSME	q_e , cal (mg/g)	k_2 ($\text{g mg}^{-1} \text{min}^{-1}$)	RMSE
30 °C	25	22.32	21.02	0.0167	1.49	19.23	0.0017	2.54
	50	44.13	43.57	0.0241	1.07	39.35	0.0010	3.68
	100	85.78	77.84	0.0132	7.46	69.62	0.0003	2.55
	200	158.46	135.30	0.0107	5.25	120.35	0.0001	6.01
	250	189.44	154.06	0.0093	4.81	137.31	0.0001	7.20
	300	214.52	162.07	0.0078	2.77	144.75	0.0001	11.21
	Average				3.81			5.53
40 °C	25	21.71	20.83	0.0178	0.64	18.47	0.0015	2.16
	50	42.81	42.25	0.0241	0.80	38.21	0.0011	3.20
	100	84.46	76.26	0.0130	7.30	68.24	0.0003	2.58
	200	157.14	134.21	0.0107	6.87	119.65	0.0001	6.08
	250	188.12	152.34	0.0092	4.55	135.76	0.0001	7.45
	300	203.86	158.33	0.0083	3.59	140.78	0.0001	12.68
	Average				3.96			5.69
50 °C	25	21.68	20.75	0.0175	0.70	18.44	0.0015	2.23
	50	41.60	41.27	0.0268	2.00	37.02	0.0011	2.50
	100	80.31	73.36	0.0136	5.98	64.25	0.0003	2.72
	200	155.42	129.38	0.0099	4.46	118.04	0.0001	7.47
	250	175.48	158.52	0.0130	6.98	124.16	0.0001	21.17
	300	188.97	167.54	0.0121	5.21	127.39	0.0001	26.97
	Average				4.22			10.57

Table 5. Thermodynamic parameters.

Temperature (K)	ΔH° (kJ/mol)	ΔS° (kJ/mol K)	Ea (kJ/mol)	ΔG° (kJ/mol)
303.15				-24.62
313.15	-2.57	0.07	10.16	-25.35
323.15				-26.08

RBBR molecules gained more kinetic energy at higher solution temperatures, escaping the active sites and decreasing adsorption capacity. Langmuir adsorption constant, K_L decreased from $0.02755 \text{ l mg}^{-1}$ at 30°C to $0.02585 \text{ l mg}^{-1}$ at 50°C , signifying that adsorption of RBBR onto MAC was favored at lower temperatures (Yusop *et al* 2021). The heterogeneity factor, n , obtained for all temperature ranges studied, was between 1.79 and 1.94, which lies between 1 and 10, confirming the favorability of the adsorption process (Yusop *et al* 2022a).

3.4. Adsorption kinetic

The nonlinear plots of the kinetic models utilized in this study, namely, PFO and PSO, are shown in figures 7 and 8, respectively, and their corresponding parameters are listed in table 4. The kinetic data were best represented by PFO because it had a lower RSME value (<4.22) than PSO (<10.57) did for all adsorption temperature ranges studied. The PFO model suggested that the sorption of RBBR onto MAC was influenced by the physisorption type of forces, which is verified in the thermodynamic study in section 3.5. Similar results, where the adsorption process was best fitted by PFO, can be observed in the adsorption of cationic dyes by Schiff's base chitosan-glutaraldehyde/AC composite (Jawad *et al* 2021a) and methylene blue dye adsorption by KOH-activated dragon fruit peel-based AC (Jawad *et al* 2021b). A decreasing trend in k_1 values from 0.0167 to 0.0078 min^{-1} , from 0.0178 to 0.0083 min^{-1} , and from 0.0175 to 0.0121 min^{-1} for solution temperatures of 30, 40, and 50°C , respectively, was observed as the initial concentration increased from 25 to 300 mg/l. The reason for this trend is that the higher the initial concentration, the higher the degree of competition between RBBR molecules to be adsorbed by the active sites on MAC; therefore, the rate constant for the adsorption process decreased. Boyd plots were constructed to understand the diffusion process involved in the RBBR-MAC adsorption system (figure 9). The Boyd plot is useful for determining the slowest step of the adsorption process. All lines in the Boyd plots (25 to 300 mg l^{-1}) did not pass through the origin, signifying that film diffusion was the rate-limiting step in the adsorption process.

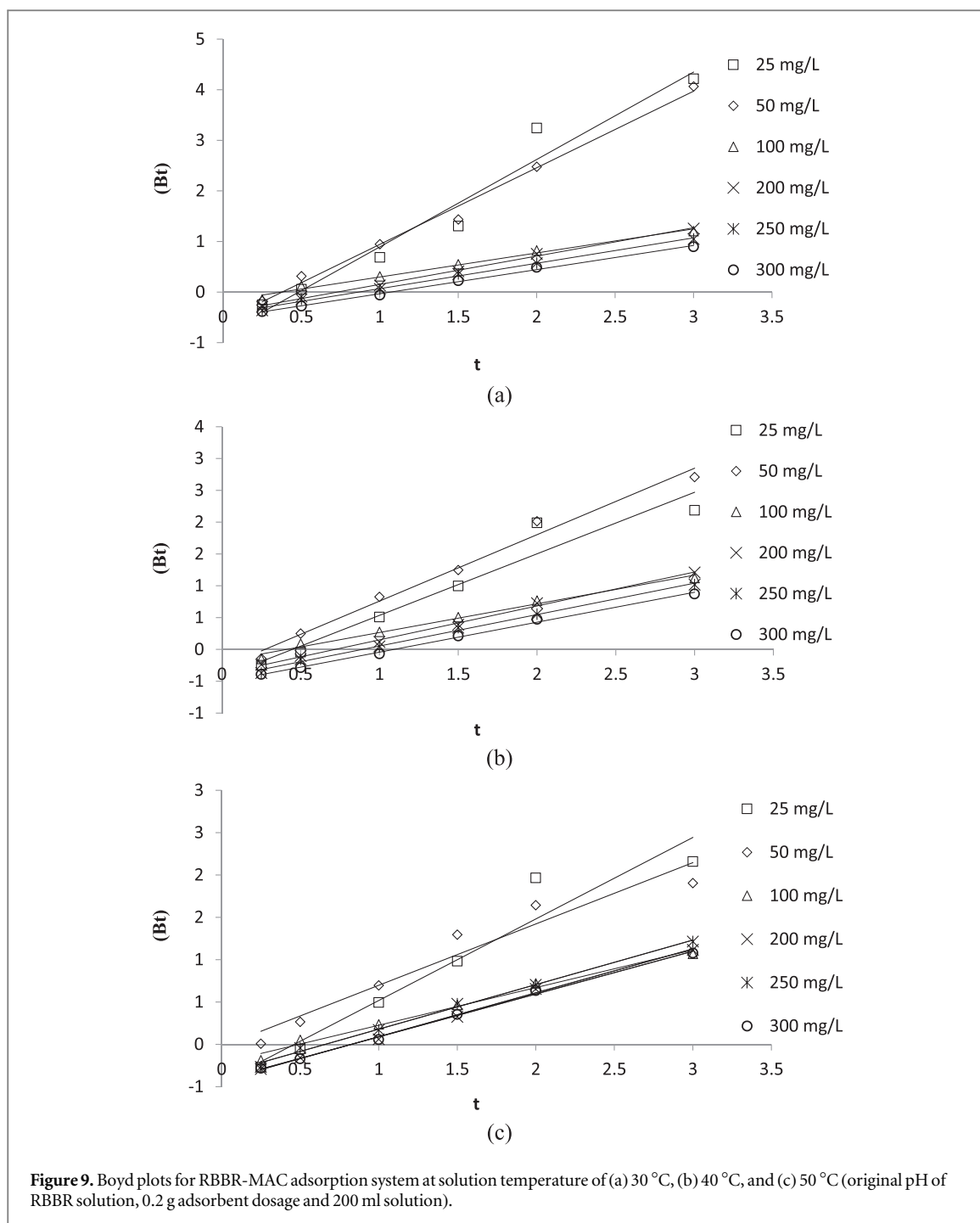
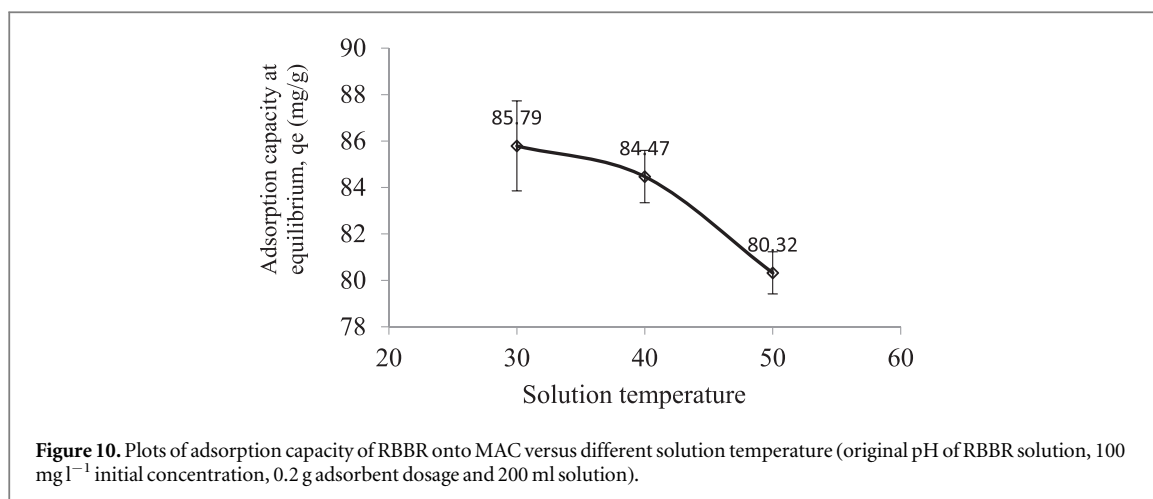


Figure 9. Boyd plots for RBBR-MAC adsorption system at solution temperature of (a) 30 °C, (b) 40 °C, and (c) 50 °C (original pH of RBBR solution, 0.2 g adsorbent dosage and 200 ml solution).

3.5. Adsorption thermodynamic

The parameters obtained from the thermodynamic study are presented in table 5, and the plot of the adsorption capacity of RBBR at equilibrium versus different solution temperatures is shown in figure 9. Based on figure 10, a decrease in the adsorption capacity of RBBR from 85.79 to 80.32 mg g⁻¹ as the solution temperature increased from 30 to 50 °C was observed, signifying the adsorption process behaved exothermically. This result was verified again by the negative value obtained for ΔH° of -2.57 kJ mol⁻¹. The exothermic nature of the adsorption process was also observed in the removal of methylene blue dye by arginine-based composite AC (Naushad *et al* 2019). Negative values of ΔG° , which are between -24.62 and -26.08 kJ mol⁻¹, signified that the adsorption of RBBR onto MAC was spontaneous in nature. The value of ΔS° was 0.07 kJ mol⁻¹. K, and this positive value indicates that the degree of randomness increased at the liquid-solid interface. This was due to the enhanced desorption of water molecules from the MAC surface owing to RBBR adsorption (Preeti *et al* 2021). The E_a value was 10.16 kJ mol⁻¹. Because this value is below 40 kJ mol⁻¹, it implies that the adsorption process was controlled by physisorption (Preeti *et al* 2021). This result is consistent with the predictions presented in section 3.4.



4. Conclusion

MAC was successful in adsorbing RBBR dye, with an adsorption capacity of 303.14 mg g⁻¹. Average pore diameter and BET surface for MAC were revealed to be 2.51 nm (mesopores) and 641.23 m² g⁻¹, respectively. The zeta potential value was determined to be -0.783 mV, which confirmed that the MAC surface was negatively charged. A low initial concentration of RBBR (25–50 mg l⁻¹) achieved equilibrium after 3 h, and high concentrations (100–300 mg l⁻¹) attained the same state after 7 h. Removal of RBBR by MAC achieved optimum value at pH 3 with 96.69 mg g⁻¹ and a solution temperature of 30 °C of 85.79 mg g⁻¹. Isotherm and kinetic studies revealed that the adsorption process was best represented by the Langmuir and PFO models. Thermodynamic parameters were calculated to be -2.57, 0.07, 10.16, and -24.62 kJ mol⁻¹ for ΔH° , ΔS° , E_a , and ΔG° , respectively; thus, the adsorption process was exothermic in nature, increasing randomness at the liquid-solid interface, governed by physisorption and spontaneous in nature.

Acknowledgments

This project was funded by the National Plan for Science, Technology and Innovation (MAARIFAH), King Abdulaziz City for Science and Technology, Kingdom of Saudi Arabia, Award Number (13-ENV1102-02).

Data availability statement

The data that support the findings of this study are available upon reasonable request from the authors.

Declarations

Competing interest

The authors report there are no competing interests to declare.

ORCID iDs

Hattan A Alharbi  <https://orcid.org/0000-0003-3297-729X>

Khaled D Alotaibi  <https://orcid.org/0000-0002-2384-1705>

References

- Ahammad N A, Yusop M F M, Din A M and Ahmad M A 2021 Preparation of *Alpinia galanga* stem based activated carbon via single-step microwave irradiation for cationic dye removal *Sains Malaysiana* **50** 2251–69
- Ahmad M A, Eusoff M A, Oladoye P O, Adegoke K A and Bello O S 2020 Statistical optimization of Remazol brilliant blue R dye adsorption onto activated carbon prepared from pomegranate fruit peel *Chemical Data Collections* **28** 100426

- Ahmad M A, Hamid S R A, Yusop M F M and Aziz H A 2017 Optimization of microwave-assisted durian seed based activated carbon preparation conditions for methylene blue dye removal *AIP Conf. Proc.* **1892** 040019
- Ahmad M A, Yusop M F M, Awang S, Yahaya N K E M, Rasyid M A and Hassan H 2021 Carbonization of sludge biomass of water treatment plant using continuous screw type conveyer pyrolyzer for methylene blue removal *IOP Conf. Ser.: Earth Environ. Sci.* **765** 012112
- Aichour A, Zaghouane-Boudiaf H and Djafer Khodja H 2022 Highly removal of anionic dye from aqueous medium using a promising biochar derived from date palm petioles: characterization, adsorption properties and reuse studies *Arabian J. Chem.* **15** 103542
- Aldawsari A M, Alsohaimi I H, Hassan H M A, Berber M R, Abdalla Z E A, Hassan I, Saleh E A M and Hameed B H 2020 Activated carbon/MOFs composite: AC/NH₂-MIL-101(Cr), synthesis and application in high performance adsorption of p-nitrophenol *Journal of Saudi Chemical Society* **24** 693–703
- Aziz A, Nasehir Khan M N, Mohamad Yusop M F, Mohd Johan Jaya E, Tamar Jaya M A and Ahmad M A 2021 Single-stage microwave-assisted coconut-shell-based activated carbon for removal of dichlorodiphenyltrichloroethane (DDT) from aqueous solution: optimization and batch studies *International Journal of Chemical Engineering* **2021** 9331386
- Brazil T R, Gonçalves M, Junior M S O and Rezende M C 2022 Sustainable process to produce activated carbon from Kraft lignin impregnated with H₃PO₄ using microwave pyrolysis *Biomass Bioenergy* **156** 106333
- Canales-Flores R A and Prieto-García F 2020 Taguchi optimization for production of activated carbon from phosphoric acid impregnated agricultural waste by microwave heating for the removal of methylene blue *Diam. Relat. Mater.* **109** 108027
- Daoud M, Benturki O, Kecira Z, Girods P and Donnot A 2017 Removal of reactive dye (BEZAKTIV Red S-MAX) from aqueous solution by adsorption onto activated carbons prepared from date palm rachis and jujube stones *J. Mol. Liq.* **243** 799–809
- Freundlich H M F 1906 Over the adsorption in solution *J. Phys. Chem.* **57** 385–471
- Guo G, Tian F, Zhang L, Ding K, Yang F, Hu Z, Liu C, Sun Y and Wang S 2020 Effect of salinity on removal performance in hydrolysis acidification reactors treating textile wastewater *Bioresour. Technol.* **313** 123652
- Han Q, Wang J, Goodman B A, Xie J and Liu Z 2020 High adsorption of methylene blue by activated carbon prepared from phosphoric acid treated eucalyptus residue *Powder Technol.* **366** 239–48
- Hijab M, Parthasarathy P, Mackey H R, Al-Ansari T and Mckay G 2021 Minimizing adsorbent requirements using multi-stage batch adsorption for malachite green removal using microwave date-stone activated carbons *Chemical Engineering and Processing - Process Intensification* **167** 108318
- Ho Y S and Mckay G 1998 Sorption of dye from aqueous solution by peat *Chem. Eng. J.* **70** 115–24
- Jawad A H, Abdulhameed A S, Wilson L D, Hanafiah M A K M, Nawawi W I, Allothman Z A and Rizwan Khan M 2021a Fabrication of Schiff's base chitosan-glutaraldehyde/activated charcoal composite for cationic dye removal: optimization using response surface methodology *Journal of Polymers and the Environment* **29** 2855–68
- Jawad A H, Saud Abdulhameed A, Wilson L D, Syed-Hassan S S A, Allothman Z A and Rizwan Khan M 2021b High surface area and mesoporous activated carbon from KOH-activated dragon fruit peels for methylene blue dye adsorption: optimization and mechanism study *Chinese Journal of Chemical Engineering* **32** 281–90
- Lagergren S K 1898 About the theory of so-called adsorption of soluble substances *Kungliga Svenska Vetenskapsakademiens Handlingar* **24** 1–39
- Langmuir I 1918 The adsorption of gases on plane surfaces of glass, mica and platinum *JACS* **40** 1361–403
- Lima E C, Hosseini-Bandegharai A, Moreno-Piraján J C and Anastopoulos I 2019 A critical review of the estimation of the thermodynamic parameters on adsorption equilibria. wrong use of equilibrium constant in the Van't Hoof equation for calculation of thermodynamic parameters of adsorption *J. Mol. Liq.* **273** 425–34
- Mahapatra U, Chatterjee A, Das C and Manna A K 2021 Adsorptive removal of hexavalent chromium and methylene blue from simulated solution by activated carbon synthesized from natural rubber industry biosludge *Environmental Technology & Innovation* **10** 1427
- Marrakchi F, Hameed B H and Bouaziz M 2020 Mesoporous and high-surface-area activated carbon from defatted olive cake by-products of olive mills for the adsorption kinetics and isotherm of methylene blue and acid blue 29 *J. Environ. Chem. Eng.* **8** 104199
- Maršálek R and Švidrnich M 2020 The adsorption of amitriptyline and nortriptyline on activated carbon, diosmectite and titanium dioxide *Environmental Challenges* **1** 100005
- Melliti A, Srivastava V, Kheriji J, Sillanpää M and Hamrouni B 2021 Date palm fiber as a novel precursor for porous activated carbon: optimization, characterization and its application as tylosin antibiotic scavenger from aqueous solution *Surfaces and Interfaces* **24** 101047
- Mohamad F M Y, Aziz A and Azmier Ahmad M 2022 Conversion of teak wood waste into microwave-irradiated activated carbon for cationic methylene blue dye removal: optimization and batch studies *Arabian J. Chem.* **15** 104081
- Naushad M, Alqadami A A, Allothman Z A, Alsohaimi I H, Algamdi M S and Aldawsari A M 2019 Adsorption kinetics, isotherm and reusability studies for the removal of cationic dye from aqueous medium using arginine modified activated carbon *J. Mol. Liq.* **293** 111442
- Omoriyekomwan J E, Tahmasebi A, Dou J, Wang R and Yu J 2021 A review on the recent advances in the production of carbon nanotubes and carbon nanofibers via microwave-assisted pyrolysis of biomass *Fuel Process. Technol.* **214** 106686
- Preeti, Banerjee S, Debnath A and Singh V 2021 Gum ghatti-alginate hybrid bead derived titania spheres for deep removal of toxic dye Remazol Brilliant Violet from aqueous solutions *Environmental Nanotechnology, Monitoring & Management* **15** 100459
- Raj A, Yadav A, Rawat A P, Singh A K, Kumar S, Pandey A K, Sirohi R and Pandey A 2021 Kinetic and thermodynamic investigations of sewage sludge biochar in removal of Remazol brilliant blue R dye from aqueous solution and evaluation of residual dyes cytotoxicity *Environmental Technology & Innovation* **23** 101556
- Sharma J, Sharma S and Soni V 2021 Classification and impact of synthetic textile dyes on aquatic flora: a review *Regional Studies in Marine Science* **45** 101802
- Varjani S, Rakholiya P, Ng H Y, You S and Teixeira J A 2020 Microbial degradation of dyes: an overview *Bioresour. Technol.* **314** 123728
- Yusop M F M, Ahmad M A, Rosli N A, Gonawan F N and Abdullah S J 2021 Scavenging malachite green dye from aqueous solution using durian peel based activated carbon *Malaysian Journal of Fundamental and Applied Sciences* **17** 95–103
- Yusop M F M, Aziz A and Ahmad M A 2022a Conversion of teak wood waste into microwave-irradiated activated carbon for cationic methylene blue dye removal: optimization and batch studies *Arabian J. Chem.* **104081**
- Yusop M F M, Aziz H A and Ahmad M A 2017 Scavenging remazol brilliant blue R dye using microwave-assisted activated carbon from acacia sawdust: equilibrium and kinetics studies *AIP Conf. Proc.* **1892**
- Yusop M F M, Jaya E M J and Ahmad M A 2022b Single-stage microwave assisted coconut shell based activated carbon for removal of Zn(II) ions from aqueous solution—optimization and batch studies *Arabian J. Chem.* **15** 104011
- Zhang H, Xing L, Liang H, Ren J, Ding W, Wang Q, Geng Z and Xu C 2022 Efficient removal of Remazol Brilliant Blue R from water by a cellulose-based activated carbon *Int. J. Biol. Macromol.* **207** 254–62